HHS Public Access

Author manuscript

Biochim Biophys Acta Mol Basis Dis. Author manuscript; available in PMC 2020 June 01.

Published in final edited form as:

Biochim Biophys Acta Mol Basis Dis. 2019 June 01; 1865(6): 1170–1181. doi:10.1016/j.bbadis.2019.01.011.

Deficiency of mouse mast cell protease 4 mitigates cardiac dysfunctions in mice after myocardium infarction

Yunzhe Wang[#a,b], **Cong-Lin Liu**[#a,b], **Wenqian Fang**[b], **Xian Zhang**[b], **Chongzhe Yang**[b], **Jie Li**[b], **Jing Liu**[b], **Galina K. Sukhova**[b], **Michael F. Gurish**[b], **Peter Libby**[b], **Guo-Ping Shi**[a,b], and **Jinying Zhang**[a]

[a]Department of Cardiology, the First Affiliated Hospital of Zhengzhou University, Key Laboratory of Cardiac Injury and Repair of Henan Province, Zhengzhou University, Zhengzhou, 450000, China

[b]Department of Medicine, Brigham and Women's Hospital and Harvard Medical School, Boston, MA 02115, USA

[#] These authors contributed equally to this work.

Abstract

Mouse mast cell protease-4 (mMCP4) is a chymase that has been implicated in cardiovascular diseases, including myocardial infarction (MI). This study tested a direct role of mMCP4 in mouse post-MI cardiac dysfunction and myocardial remodeling. Immunoblot and immunofluorescent double staining demonstrated mMCP4 expression in cardiomyocytes from the infarct zone from mouse heart at 28 days post-MI. At this time point, mMCP4-deficient *Mcpt4*$^{-/-}$ mice showed no difference in survival from wild-type (WT) control mice, yet demonstrated smaller infarct size, improved cardiac functions, reduced macrophage content but increased T-cell accumulation in the infarct region compared with those of WT littermates. mMCP4-deficiency also reduced cardiomyocyte apoptosis and expression of TGF-β1, p-Smad2, and p-Smad3 in the infarct region, but did not affect collagen deposition or α-smooth muscle actin expression in the same area. Gelatin gel zymography and immunoblot analysis revealed reduced activities of matrix metalloproteinases and expression of cysteinyl cathepsins in the myocardium, macrophages, and T cells from *Mcpt4*$^{-/-}$ mice. Immunoblot analysis also found reduced pSmad2 and p-Smad3 in the myocardium from *Mcpt4*$^{-/-}$ mice, yet fibroblasts from *Mcpt4*$^{-/-}$ mice showed comparable levels of p-Smad2 and p-Smad3 to those of WT fibroblasts. Flow cytometry, immunoblot analysis, and immunofluorescent staining demonstrated that mMCP4-deficiency reduced the expression of

Corresponding author: Guo-Ping Shi, D.Sc., Cardiovascular Medicine, Brigham and Women's Hospital, 77 Avenue Louis Pasteur, NRB-7, Boston, MA 02115, USA, Tel.: 617-525-4358, Fax: 617-525-4380, gshi@rics.bwh.harvard.edu; Jinying Zhang, PhD., Department of Cardiology, First Affiliated Hospital of Zhengzhou University, 1 Jianshe Road, Zhengzhou, Henan 450000, China, Tel.: +86 371 67967243, Fax: +86 371 67967643, jyzhang@zzu.edu.cn.

Author Contribution

GS and JZ conceived and designed the study, YW, CL, WF, XZ, CY, JLi and JLiu performed experiments, collected and analyzed data, GKS supervised histological and IHC data analysis, MFG analyzed data from mouse model, YW, PL, and GS wrote the manuscript.

Conflict of interest: The authors have declared no conflicts of interest.

proapoptotic cathepsins in cardiomyocytes and protected cardiomyocytes from H_2O_2-induced apoptosis. This study established a role of mMCP4 in mouse post-MI dysfunction by regulating myocardial protease expression and cardiomyocyte death without significant impact on myocardial fibrosis or survival post-MI in mice.

Keywords

mMCP4; myocardial infarction; cardiomyocyte; fibroblast; apoptosis; fibrosis

1. Introduction

Accumulating evidence suggests a role of mast cells in cardiovascular diseases (CVD) [1]. Distinct from most other inflammatory cells, mast cells contain a set of signature serine proteases, including chymase, tryptase, and carboxypeptidase A [2,3]. These enzymes hydrolyze extracellular matrix (ECM) proteins and cell surface proteins, activate pro-enzymes [2], and generate angiotensin-II (Ang-II) [4]. Chymase and tryptase can directly degrade collagens and interrupt the structural integrity of the arterial wall. Chymase also cleaves apoA-I to destroy its activity in suppressing NF-κB-dependent coronary artery endothelial cell (EC) expression of VCAM-1 (vascular cell adhesion molecule-1) and monocyte adhesion [5]. Chymase-mediated production of Ang-II in cardiovascular tissues [6,7] activates macrophage expression of MCP-1 (monocyte chemoattractant protein-1), a chemokine implicated in monocyte recruitment [8]. Chymase and tryptase also activate matrix metalloproteinases (MMPs) MMP-1, MMP-3 and MMP-9 [9,10] and TGF-β [11,12] that contribute to arterial wall ECM degradation or synthesis.

In patients with myocardial infarction (MI), myocardial chymase activity increased at 14–21 days post-MI [13], suggesting a role of chymase in a later phase post-MI myocardial remodeling. Chymase functions in CVD have undergone thorough testing using chymase inhibitors and chymase-deficient mice. In hamsters, chymase inhibition suppressed myocardial fibrosis in hypertensive cardiac hypertrophy [14] and inhibited diet-induced atherosclerosis [15]. In rodent MI, chymase inhibitors suppressed ischemic remodeling, reduced cardiac hypertrophy and dysfunctions following coronary artery ligation, and extended survival [16–20] in company with reduced expression of collagen I/III due to the suppression of chymase-activated TGF-β [20]. In dogs with ischemia/reperfusion injury, chymase increases in cardiomyocytes. In cultured HL-1 cardiomyocytes, addition of chymase induced cell death [21].

Mouse mast cell protease-4 (mMCP4) is the functional homolog of human chymase [16]. We reported that mMCP4-deficiency in *Mcpt4*$^{-/-}$ mice attenuated AAA growth and reduced lesion numbers of inflammatory cells, smooth muscle cell apoptosis, ECM degradation, and angiogenesis [22]. A recent study using *Mcpt4*$^{-/-}$ mice tested this enzyme's role in ischemia/reperfusion-induced cardiac dysfunction and myocardial remodeling. The expression of mMCP4 rose in the hearts with increased tryptase^{+} mast cells 72 hours after reperfusion. Cardiomyocytes surface showed diffused mMCP4 expression. Two weeks after reperfusion, *Mcpt4*$^{-/-}$ mice showed significantly reduced scar size, better preserved left

ventricular (LV) ejection fraction (EF), reduced LV dilatation, decreased end-systolic and end-diastolic volumes and reduced infarct expansion, compared to WT control mice. *Mcpt4*$^{-/-}$ mice also showed reduced cardiomyocyte hypertrophy in the remote LV and LV fibrosis, although mMCP4-deficiency did not affect blood pressure [23]. It was suggested that mMCP4 contributed to ischemia/reperfusion-induced cardiac dysfunction by degrading insulin growth factor IGF-1 [23], a putative cardioprotective factor in the setting of permanent coronary artery occlusion or of ischemia/reperfusion [24].

This study performed permanent coronary artery ligation in mice and found that mMCP4-deficiency significantly improved post-MI cardiac function, but did not affect LV volume and LV internal diameter end diastole and end systole, post-MI myocardium fibrosis, or survival. Mechanistic study demonstrated the participation of mMCP-4 in cardiomyocyte apoptosis, but no effect on TGF-β signaling in cardiac fibroblasts.

2. Materials and methods

2.1 Mouse MI

Male mMCP-4-deficient *Mcpt4*$^{-/-}$ mice (C57BL/6J, N10) [22] and their WT littermates underwent experimental MI at 8~10 weeks of age as described [25]. After anesthesia with isoflurane (1.5%) and a volume-controlled ventilator (Harvard Apparatus, Holliston, MA), the heart was exposed by a left thoracotomy and the left anterior descending (LAD) artery ligated with a 7–0 silk suture (Ethicon, Somerville, NJ). Blanching of the distal myocardium verified ischemia. Sham-operated mice underwent the same procedure without LAD ligation. Mice were give one dose of buprenorphine at 0.05–0.1 mg/kg by subcutaneous injection before the surgery. Mice were then anesthetized under introductory 4% isoflurane inhalation and then 1.5% isoflurane maintenance during the surgical procedure. Mice received one dose of buprenorphine at 0.05–0.1 mg/kg by subcutaneous injection at each 12 hours after the surgery and one dose of meloxicam at 3–5 mg/kg by subcutaneous injection at each 24 hours for 48 hours. Mice were sacrificed at 3 days or 28 days post-MI for further studies. At harvest, mice were euthanized by delivering 100% CO_2 for a minimum of 3 min from a pressurized system at 5 lb/in. into a sealed cage. All animal procedures conformed to the Guide for the Care and Use of Laboratory Animals published by the US National Institutes of Health and was approved by the Brigham and Women's Hospital Standing Committee on Animals (protocol #2016N000289).

2.2 Echocardiography

Transthoracic two-dimensional (2D) parasternal short axis M-mode echocardiogram was performed at baseline and at 28 days post-MI, using the Vevo 2100 system (VisualSonics, Toronto, Canada) with a 30-MHz transducer. Mice were positioned and restrained on a 37°C heating pad without anesthesia. M-mode tracings at the mid-papillary muscle level were recorded to measure LV wall thickness, end-diastolic diameter (LV EDD) and end-systolic diameter (LV ESD). Percentage of fraction shortening (%FS) and %EF were calculated by the manufacturer's software package.

2.3 Morphometric analysis

Mouse heart weights were recorded when excised after termination. LV was divided from apex to base into three cross sections, and the medium section was embedded in OCT compound (Sakura Finetek, Torrance, CA). The infarct size was determined from hematoxylin-eosin stained sections 3 days and 28 days post-MI.

2.4 Immunofluorescent, immunohistological, and Masson's trichrome staining

To localize apoptotic cells and detect the expression of mMCP4 in the heart, heart frozen sections (6 μm) were used for immunofluorescent staining for cardiomyocyte (myosin heavy chain, 1:50, Cat# bs-15444R-A488, Bioss In. Woburn, MA), fibroblast (α-smooth muscle actin α-SMA, 1:500, Cat# F3777, Sigma-Aldrich, St Louis, MO, USA), macrophage (Mac-2, 1:100, Cat# CL8942LE, Cedarlane, Burlington, Ontario, Canada), cleaved caspase-3 (1:100, Cat# 8172, Cell Signaling Technology, Danvers, MA), and mMCP4 (1:200) [26]. Alexa Fluor 488 (1:300, Cat# A-21208, Thermo Fisher Scientific, Waltham, MA) or Alexa Fluor 555 (1:500, Cat# A-21428, Thermo Fisher Scientific) was used as the secondary antibody. Cell nuclei were counterstained with DAPI (4′,6-diamidino-2-phenylindole, 1:10, Cat# R37606, Thermo Fisher Scientific). Images were collected under an Olympus FluoView™ FV1000 confocal microscope. Heart frozen sections (6 μm) were also stained for macrophage (Mac-3, 1:900, Cat# 553322, BD Biosciences, San Jose, CA), $CD4^+$ T-cell (CD4, 1:90, Cat# 553043, BD Biosciences), $CD8^+$ T-cell (CD8, 1:100, Cat# 14–0081-85, eBioscience, San Diego, CA), α-SMA (1:750, Cat# 14968s, Cell Signaling Technology), TGF-β1 (1:100, Cat# MAB532, R&D Systems, Minneapolis, MN), p-Smad2 (1:100, Cat# AB3849, EMD Millipore, Billerica, MA), and p-Smad3 (1:25, Cat# ab52903, Abcam, Cambridge, MA). Apoptotic cells were detected using ApopTag® Plus Peroxidase In Situ Apoptosis Detection Kit according to the manufacturer's instructions (Cat# S7100, EMD Millipore). Apoptotic nuclei were defined as TUNEL (Terminal deoxynucleotidyl transferase dUTP nick end labeling)-positive nuclei in cells with morphological features of apoptotic cell death (cell shrinkage, aggregation of chromatin into dense masses, and cell fragmentation) [27]. Masson's trichrome kit was used to detect heart collagen deposition according to the manufacturer's instruction (Cat# 87019, Thermo Fisher Scientific). A virtual slide microscope (VS120, Olympus, Center Valley, PA, USA) was used to capture images. The staining area was measured using computer-assisted image quantification (Image-Pro Plus software, Media Cybernetics, Rockville, MD, USA), and immunopositive cells were counted manually. One scientist was responsible to complete the measurement and data analysis of each variable to avoid possible interpersonal variation. All mouse experiments were performed, and data were analyzed in a blinded fashion by at least 3 observers.

2.5 Quantitative real-time polymerase chain reaction (RT-PCR).

RT-PCR was used to determine the expression of T-bet, Gata-3, RORγt, Foxp3, MMP-2, MMP-9, tissue inhibitor of metalloproteinase-1 (TIMP-1), collagen I, collagen III, myosin heavy chain-6 (myosin-6), myosin-7, and natriuretic peptide precursor A (NPPA) in heart tissues. Total RNA was prepared using TRIzol reagent according to the manufacturer's recommendations (Cat# 15596018, Thermo Fisher Scientific). RNA concentration and

quality were evaluated using the Agilent 2100 bioanalyzer (Nano LabChip, Agilent Technologies, Santa Clara, CA). β-actin was used as endogenous control. Results were expressed as fold of change relative to the control cell as the baseline.

2.6 Cell culture

Macrophages were prepared by differentiating bone marrow cells from *Mcpt4*$^{-/-}$ and WT mice in macrophage colony-stimulating factor (M-CSF) (20 ng/ml, Cat# 416-ML-050, R&D Systems) for 10 days. Total T cells were separated from splenocytes using a nylon-wool column (Cat# 21759, Polysciences, Inc., Warrington, PA) to yield a crude T cell preparation. $CD4^+$ and $CD8^+$ T cells were prepared as described previously [28]. Macrophages, $CD4^+$ and $CD8^+$ T cells were cultured in RPMI containing 10% fetal bovine serum (FBS) and 1% penicillin/streptomycin.

Adult cardiomyocytes from *Mcpt4*$^{-/-}$ and WT mice were isolated and cultured as previously reported [29,30]. After centrifugation at 20 g for 5 minutes, cardiac fibroblasts in the supernatant were collected and cultured in high-glucose DMEM medium (Cat# 10566016, Invitrogen, Carlsbad, CA) containing 10% FBS and 1% penicillin/streptomycin. And the remaining pellet of cardiomyocytes was re-suspended in MEM containing 1% BSA, 1% penicillin/streptomycin and 10 mM 2,3-Butanedione monoxime (BDM) (Cat# B0753, Sigma-Aldrich). The medium was changed every 48 hours.

2.7 Fibroblast trans-differentiation

Adult mouse cardiac fibroblasts from *Mcpt4*$^{-/-}$ and WT mice were incubated in DMEM containing 1% FBS for 24 hours. Cells were then treated with recombinant mouse TGF-β1 (10 ng/mL, Cat# 14–8342-80, eBioscience) in DMEM containing 1% FBS for 30 minutes or 24 hours. Cells were lysed in RIPA lysis buffer (Cat# BP-115, Boston Bio-products, Ashland, MA) supplemented with a protease and phosphatase inhibitor cocktail (Cat# 78442, Thermo Fisher Scientific) for western blot analysis to detect p-Smad2, p-Smad3, and α-SMA.

2.8 In situ zymography

Heart tissue, macrophage, and T-cell MMP activities were assessed using gelatin gel zymography as described previously [31]. Briefly, 20 μg heart tissue, macrophage, or T-cell lysate was subjected to an 8% SDS-PAGE. Gel was then incubated in 2.5% Triton X-100 for 90 minutes to remove SDS, followed by incubation for 36 hours in a developing buffer containing 50 mmol/L Tris-HCl, 0.2 mol/L NaCl, 5 mmol/L $CaCl_2$, and 0.02% Brij-35 pH7.6. Gel was then stained in a staining buffer containing 0.1% Coomassie blue R-250 (Cat# 1610400, Bio-Rad, Hercules, CA), 30% methanol, and 10% glacial acetic acid, and destained for 2 hours in a destaining buffer containing 30% methanol and 10% acetic acid.

2.9 Western blot

For immunoblot analysis, an equal amount of protein lysate from each cell type preparation or myocardium tissue extract was separated by SDS-PAGE, blotted, and detected with different antibodies, including cathepsin K (CatK) (1:1000, Cat# PB9856, BOSTER, Pleasanton, CA), cathepsin S (CatS) (1:1000) [32], cathepsin B (CatB) (1:1000, Cat# PC41–

100UG, Sigma-Aldrich), cathepsin L (CatL) (1:1000, Cat# 168–10557, RayBiotech, Inc., Norcross, GA), mMCP4 (1:1000), α-SMA (1:1000, Cat# 14968s, Cell Signaling Technology), GAPDH (1:1000, Cat# 2118S, Cell Signaling Technology), p-Smad2 (1:1000, Cat# 3101s, Cell Signaling Technology), p-Smad3 (1:1000, Cat# 9520s, Cell Signaling Technology), importin-β (1:1000, Cat# 8673S, Cell Signaling Technology) and RanBP3 (1:1000, Cat# SC-373678, Santa Cruz Biotechnology, Dallas, TX), α-actin (1:1000, Cat# A5441-.2ML, Sigma-Aldrich), and histone-H3 (1:1000, Cat# ab1791, Abcam).

2.10 Cardiomyocyte apoptosis, flow cytometry, immunofluorescent, and immunoblot analysis

Cardiomyocytes from *Mcpt4*$^{-/-}$ and WT mice were treated with or without 100 μM H_2O_2 for 4 hours before harvest. Cell apoptosis was detected using the FITC annexin V apoptosis detection kit (Cat# 556547, BD Biosciences), followed by FACS analysis to detect annexin V and propidium iodide (PI) reactivity. This test discriminates between intact cells (annexin V^-/PI^-), early apoptotic cells (annexin V^+/PI^-), and late apoptotic cells (annexin V^+/PI^+). Apoptotic cardiomyocytes were also examined using immunofluorescent double staining with annexin V (1:100, Cat# PA5–27872, Thermo Fisher Scientific) and PI (Cat# P3566, Thermo Fisher Scientific). Alexa Fluor 488 (1:500, Cat# A-11008, Thermo Fisher Scientific) was used as the secondary antibody. The cell nuclei were counterstained with DAPI (1:10, Cat# R37606, Thermo Fisher Scientific). Images were captured using the Olympus FluoView™ FV1000 confocal microscope. The integrated intensities of annexin V and PI in staining areas were measured using computer-assisted image quantification system (ImageJ software, National Institutes of Health). Cardiomyocytes treated with and without H_2O_2 for 4 hours were also lysed in RIPA lysis buffer (Cat# BP-115, Boston Bio-products) supplemented with a protease and phosphatase inhibitor cocktail (Cat# 78442, Thermo Fisher Scientific) to detect the production of Bax (1:1000, Cat# 2772s, Cell Signaling Technology), Bid (1:500, Cat# MAB860, R&D Systems), and tBid by immunoblot analysis.

2.11 Isolation of nuclear and cytoplasmic extract

The nuclear extraction was prepared using an NE-PER nuclear cytoplasmic extraction reagent kit (Cat# 78833, Thermo Fisher Scientific) according to the manufacturer's instruction. Briefly, cardiac fibroblasts from *Mcpt4*$^{-/-}$ and WT mice were suspended in 200 μl of cytoplasmic extraction reagent-I and incubated on ice for 10 min followed by addition of 11 μl of a second cytoplasmic extraction reagent-II. After centrifugation, the supernatant fraction (cytoplasmic extract) was transferred to a pre-chilled tube. The insoluble pellet fraction, which contains crude nuclei, was re-suspended in 100 μl of a nuclear extraction reagent. After centrifugation, the resulting supernatant, constituting the nuclear extract, was used for the western blot to detect p-Smad2, p-Smad3, GAPDH, and histone-H3.

2.12 Statistical analysis

All mouse data were expressed as mean ± SEM. Shapiro-Wilk test was used to determined data distribution normality. Log-transformation was used for data that were not normally distributed after the primary normality test. Independent *t*-test was used for comparison between two groups. One-way ANOVA with post-hoc Bonferroni test was used for comparison among three or more groups. Kaplan-Meier survival analysis with log-rank test

was used to compare survival rates between groups. SPSS 22.0 was used for analysis, and $P < 0.05$ was considered statistically significant.

3. Results

3.1 Deficiency of mMCP4 improves cardiac function after coronary artery ligation

In humans, chymase peaks in the myocardium at 2~3 weeks after MI [13]. We produced MI in mice and assessed mMCP4 expression in the heart at 28 days post-MI. Immunoblot analysis revealed elevated mMCP4 expression in heart from mice with MI, compared with that from sham-operated mice (Figure 1A). Although chymase is thought a mast cell serine protease [2,3], immunofluorescent double staining revealed mMCP4 expression in myosin heavy chain-positive cardiomyocytes in the infarct and border zones from mouse heart at 28 days post-MI. In contrast, cardiomyocytes from the remote region showed negligible mMCP4 expression (Figure 2B). At a much lower level, some α-SMC-positive cardiac fibroblasts and Mac-2-positive macrophages in the infarct regions also express mMCP4 (Figure 1C). Prior studies in stroke-prone spontaneously hypertensive rats [33] and in rodent MI [16–20] showed that chymase inhibition prolonged survival. When mMCP4-deficient *Mcpt4*$^{-/-}$ mice and their WT littermates underwent MI production, they showed no differences in survival during the course of 28 days (Figure 1D). Yet, at 28 days post-MI, mMCP4-deficiency reduced infarct size (Figure 1E) and yielded significantly increased ejection fraction (EF%) and fractional shortening (%FS) (Figure 1F-1H). Along with these improvements in cardiac function, *Mcpt4*$^{-/-}$ mice gained body weight during this 28-day post-MI although not statistically significant. WT mice lost significant body weight, although total heart weight and heart-to-body weight ratio did not differ between the two genotypes before or after MI (Figure 1I). In contrast, at 3 days post-MI, none of the 10 WT and 8 *Mcpt4*$^{-/-}$ mice died. They showed no difference in infarct size (Figure 1E), body weight, heart weight, or their ratios (data not shown), supporting a detrimental role of mMCP4 in post-MI myocardial remodeling during the 28 days post-MI. Previous study of mice with ischemia/reperfusion injury showed that mMCP4-deficiency reduced the end-systolic and end-diastolic LV volumes [23]. In mice with permanent LAD ligation, we did not detect significant differences in LV end-diastolic and end-systolic volumes (Figure 1J) or LV diastole and systole internal diameters (Figure 1K).

3.2 Deficiency of mMCP4 affects myocardium inflammatory cell content and cell apoptosis

In ischemia/reperfusion-injured hearts, mMCP4-deficiency reduced macrophage accumulation in the myocardium [23]. We also detected significantly fewer macrophages in both the infarct and remote regions from *Mcpt4*$^{-/-}$ mice than those from their WT littermates (Figure 2A/2B). However, infarct area $CD4^+$ and $CD8^+$ T-cell content was higher in *Mcpt4*$^{-/-}$ mice than in WT control mice (Figure 2C/2E), although these cells in the remote regions did not differ between the genotypes (Figure 2D/2F). RT-PCR analysis of the myocardium tissue extracts showed that the increased $CD4^+$ T cells in the *Mcpt4*$^{-/-}$ mouse hearts were mainly Gata-3-positive Th2 cells. Th1 (T-bet), Th17 (RORγt), and regulatory T cells (Foxp3) also trended higher in hearts from *Mcpt4*$^{-/-}$ mice than those in WT control mice, without reaching statistical significance (Figure 2G).

As discussed, chymase induces apoptosis of mouse cardiomyocytes HL-1 and rat neonatal cardiomyocyte [21,34]. In ischemia/reperfusion mice, mMCP4-deficiency reduced myocardium cell apoptosis [23]. TUNEL staining revealed significantly fewer apoptotic cells in the infarct region in *Mcpt4*$^{-/-}$ mouse hearts than those in WT mouse hearts (Figure 2H), but not in the remote regions (Figure 2I).

3.3 Deficiency of mMCP4 reduces myocardial TGF-β signaling but does not affect tissue fibrosis

Myocardial fibrosis affects post-MI cardiac functions. Chymase can act directly on collagen or indirectly by activating MMPs or TGF-β [9–11]. Yet, Masson's Trichrome staining (Figure 3A) or Sirius red staining (data not shown) did not detect significant differences in collagen deposition in post-MI heart infarct or remote regions between the *Mcpt4*$^{-/-}$ and WT control mice. Immunostaining of α-SMA detected fewer fibroblasts in the remote areas in *Mcpt4*$^{-/-}$ mice than those in WT control mice, but not in the infarct areas (Figure 3B). The content of TGF-β1, p-Smad2, and p-Smad3 in the infarct areas but not in the remote areas from *Mcpt4*$^{-/-}$ mice fell significantly lower compared to WT control mice (Figure 3C-3E). RT-PCR analysis of the same infarct region yielded similar conclusion. mMCP4-deficiency did not affect the expression of myocardial stress proteins myosin-6, myosin-7, and NPPA (Figure 3F) or myocardial fibrotic proteins collagen-1, collagen-III, and their protease and protease inhibitor MMP-9 and TIMP-1. Only MMP-2 expression was reduced from *Mcpt4*$^{-/-}$ mice post-MI (Figure 3G).

Low levels of TGF-β1, p-Smad2, and p-Smad3 in the infarct areas from *Mcpt4*$^{-/-}$ mice did not correlate with locally reduced collagen or α-SMA expression, suggesting that mMCP-4 effects on cardiac fibrosis did not depend on TGF-β signaling. Gelatin zymography revealed much lower MMP-9 and MMP-2 activities in post-MI heart tissue extracts from *Mcpt4*$^{-/-}$ mice than those from WT control mice (Figure 4A), suggesting their additional post-translational or activation regulation. Indeed, immunoblot analysis detected much lower levels of CatK and CatS in heart tissue extracts from *Mcpt4*$^{-/-}$ mice than those from WT control mice (Figure 4B). These cathepsins not only degrade ECM proteins, but also activate MMPs [35,36]. mMCP-4 appeared to regulate the expression and/or activation of these proteases. To test this hypothesis further, we performed both gelatin gel zymography and immunoblot analysis of macrophages, $CD4^+$ T cells, and $CD8^+$ T cells from both WT and *Mcpt4*$^{-/-}$ mice. We detected lower MMP-9 and MMP-2 activities and CatS and CatK expression in all these inflammatory cells from *Mcpt4*$^{-/-}$ mice than in those from WT control mice (Figure 4C-4F).

3.4 Deficiency of mMCP4 moderately affects fibroblast TGF-β signaling

Deficiency of mMCP4 impaired TGF-β signaling, including the TGF-β protein levels and those of p-Smad2 and p-Smad3 in the infarcted myocardium (Figure 3C-3E), but did not affect collagen or α-SMA levels in the same areas (Figure 3A/3B). Reduced MMP activity and cysteinyl cathepsin expression in myocardial extracts from *Mcpt4*$^{-/-}$ mice (Figure 4A/4B) suggest impaired ECM degradation in post-MI hearts from these mice due to the lack of mMCP4 and reduced activity or expression of MMPs and cathepsins. Yet, mMCP4-deficiency may not only reduce protease expression, activation, and ECM metabolism, but

also affect ECM synthesis. Consistent with the immunostaining results in Figure 3D/3E, immunoblot analysis also detected suppression of p-Smad2 and pSmad3 in the infarct extracts from the *Mcpt4*$^{-/-}$ mice (Figure 5A). Fibroblasts participate prominently in myocardial fibrosis following ischemic injury. Yet, fibroblasts isolated from *Mcpt4*$^{-/-}$ mice showed moderate reduction in p-Smad2 and α-SMA compared to those from WT animals. TGF-β treatment elicited comparable amounts of p-Smad3 in fibroblasts between the two genotypes (Figure 5B). After separating fibroblast nuclear and cytosol fractions, we detected no differences in either p-Smad2 or p-Smad3 in the nuclear fraction between cells from WT and *Mcpt4*$^{-/-}$ mice. GAPDH and histone-H3 antibodies were used to monitor the cytosol and nuclear protein preparations (Figure 5C). Immunoblot analysis also detected similarly increased amounts of the nuclear membrane proteins importin-β and RanBP3 that mediate p-Smad2-p-Smad3 complexes import and export through the nuclear membrane [37,38] in lysates of fibroblasts from *Mcpt4*$^{-/-}$ mice (Figure 5D). Simultaneous increases of p-Smad2-p-Smad3 complex import and export in fibroblasts from *Mcpt4*$^{-/-}$ mice may account for similar nuclear p-Smad2 and p-Smad3 contents between fibroblasts from WT and *Mcpt4*$^{-/-}$ mice (Figure 5C) and similar levels of collagen and α-SMA in the infarct areas between the two genotypes of mice (Figure 3A/3B).

3.5 Deficiency of mMCP4 promotes cardiomyocyte apoptosis

Cardiomyocyte apoptosis contributes to ischemic cardiac dysfunction [39]. Chymase promotion of apoptosis of cultured rodent cardiomyocytes [21,34] suggests that reduced apoptosis in the infarcts of *Mcpt4*$^{-/-}$ mice (Figure 2H) resulted from cardiomyocyte death. To test this hypothesis, we performed immunofluorescent double staining to detect cleaved caspase 3-positive cardiomyocytes and fibroblasts, two major cell types in the post-MI heart. We localized cleaved caspase 3-positive cells to myosin heavy chain-positive cardiomyocytes in both the infarct and border zones in post-MI hearts from WT and *Mcpt4*$^{-/-}$ mice. We detected negligible apoptosis in the remote area (Figure 6A). Cardiomyocyte apoptosis was significantly reduced in the infarct region from *Mcpt4*$^{-/-}$ mice post-MI compared to that from WT mice (Figure 6A/6B). In contrast, the infarct and border zones or the remote area in post-MI hearts from WT or *Mcpt4*$^{-/-}$ mice showed negligible α-SMA/cleaved caspase-3-positive fibroblasts with insignificant differences between the genotypes (Figure 6C/6D). These observations suggest that the apoptotic cells that we detected in the post-MI hearts in Figure 2H were mainly cardiomyocytes and that mMCP4 played an essential role in cardiomyocyte apoptosis during infarction.

To test the participation of mMCP4 in cardiomyocyte apoptosis, we isolated adult mouse cardiomyocytes from both WT and *Mcpt4*$^{-/-}$ mice and induced apoptosis by H_2O_2 treatment. As expected, H_2O_2 induced the apoptosis of cardiomyocytes from both WT and *Mcpt4*$^{-/-}$ mice. Yet, flow cytometric analysis demonstrated that both early (annexin V^+/PI^-) and late (annexin V^+/PI^+) apoptosis of cardiomyocytes from *Mcpt4*$^{-/-}$ mice fell significantly compared to WT control mice (Figure 7A/7B). Immunofluorescent double staining of annexin V and PI also revealed reduction of H_2O_2-induced early (annexin V^+PI^-) and late apoptosis (annexin V^+PI^+) of cardiomyocytes from *Mcpt4*$^{-/-}$ mice (Figure 7C/7D). H_2O_2-induced apoptosis of cardiomyocytes from WT mice often displayed morphological changes, but we hardly detected any such changes in cells from *Mcpt4*$^{-/-}$ mice (Figure 7C,

insets). Immunoblot analysis detected greatly reduced production of cell apoptosis signature molecules Bax and tBid in cardiomyocytes from *Mcpt4*$^{-/-}$ mice after H_2O_2-induced apoptosis (Figure 7E). Proteolytic activation of the pro-apoptotic tBid from Bid is mediated by cysteinyl cathepsins [36,40,41]. Immunoblot analysis detected reduction of the active CatS, CatK, CatL, and CatB in H_2O_2-treated cardiomyocytes from *Mcpt4*$^{-/-}$ mice, compared to that from WT cardiomyocytes (Figure 7F), suggesting a role of mMCP4 in promoting cardiomyocyte apoptosis in the post-MI myocardium by regulating or activating cysteinyl cathepsin expression and activation.

4. Discussion

This study used permanent ligation of the LAD coronary artery in mMCP4-deficient mice to assess a direct role of mouse chymase mMCP4 in ischemic myocardial remodeling and dysfunction. Consistent with prior studies with chymase inhibitors and mMCP4-deficient mice in ischemia/reperfusion cardiac injury, mMCP4-deficiency reduced infarct size and infarct region cardiomyocyte apoptosis and enhanced ejection fraction and fractional shortening. Deficiency of mMCP4 also reduced infarct macrophage accumulation, protease expression and activities, and TGF-β signaling, including p-Smad2 and p-Smad3 expression.

At variance with prior studies, however, this study did not show significant differences in post-MI survival and in LV volumes or LV internal diameters between WT and mMCP4-deficient *Mcpt4*$^{-/-}$ mice. Prior studies demonstrated a role of chymase in tissue fibrosis by activating TGF-β in several models of human diseases [14,20,23,42,43]. This study also found significantly reduced expression of TGF-β, p-Smad2, and p-Smad3 in the infarct in *Mcpt4*$^{-/-}$ mice, yet we did not detect significant differences in collagen deposition and α-SMA expression in the same infarct regions between mice with and without mMCP4 expression. Although the exact mechanism responsible for such discrepancies remains incompletely characterized, our observations suggest that reduced TGF-β signaling but unchanged collagen and α-SMA expression in the infarct myocardium of *Mcpt4*$^{-/-}$ mice compared with those in the WT mice result from the deficiency of mMCP4 activity and reduction of MMP-2, MMP-9, CatS, CatK, and possibly other proteases that degrade collagen, laminin, and other ECM proteins in the cardiac fibrotic tissues. This possibility is supported by the observation of reduced MMP2, MMP-9, CatS, and CatK in post-MI heart tissue extracts, purified macrophages, and $CD4^+$ and $CD8^+$ T cells from *Mcpt4*$^{-/-}$ mice. The mechanisms by which deficiency of one protease can affect the activity and/or expression of the others remain obscure [22,41,44]. We recently discovered a role of proteases in regulating TGF-β signaling by interacting with TGF-β receptors and nuclear transporter proteins (Shi unpublished observations). Chymase may play a similar role, although this study did not explore this possibility. Chymase- and cathepsin-mediated MMP activation [9,10,35] may account for reduced MMP-2 and MMP-9 activities in myocardium, macrophages, and T cells from *Mcpt4*$^{-/-}$ mice. Although it remains unknown whether chymase also activates cysteinyl cathepsins, these cathepsins activate chymase [45,46]. Therefore, these serine and cysteine proteases may interact during MI healing and contribute to post-MI cardiac fibrosis and dysfunction.

This study reported reduced TGF-β and p-Smad2 and p-Smad3 in the cardiac tissue extracts from *Mcpt4*$^{-/-}$ mice. Yet, we did not detect substantial change in amounts of p-Smad2, p-Smad3, and α-SMA in fibroblasts from these mice. Fibroblasts are the major cell type responsible for cardiac tissue fibrosis. Moderate to minimal reduction of p-Smad2, p-Smad3, and α-SMA in fibroblasts from *Mcpt4*$^{-/-}$ mice may be responsible for negligible differences in infarct area collagen and α-SMA expression between WT and *Mcpt4*$^{-/-}$ mice as well. Yet, it remains unexplained what causes reduced p-Smad2 and p-Smad3 in the whole cardiac tissue extracts from *Mcpt4*$^{-/-}$ mice. mMCP4 activity may affect TGF-β signaling in other cardiac cells such as cardiomyocytes [47,48]. Indeed, cardiomyocyte-specific TGF-β signaling affects neutrophil content in infarcts without affecting cardiac fibrosis [49].

The current study established a role mMCP4 in post-MI cardiomyocyte apoptosis in the ischemic heart, a contributor to cardiac dysfunction. Inhibition of cardiomyocyte apoptosis improves remodeling and preserves cardiac function following coronary artery ligation [50,51]. Here we provide direct evidence of mMCP4 involvement in cardiomyocyte apoptosis in post-MI myocardium in vivo and in cultured adult mouse cardiomyocytes. Deficiency of mMCP4 protected cardiomyocytes from ischemia-induced apoptosis in the myocardium and H_2O_2-induced apoptosis in cultured cells. IGF-1 inhibits cardiomyocyte apoptosis via multiple mechanisms [52,53]. Prior studies suggested a role of mMCP4 in promoting cardiomyocyte apoptosis by degrading the cardioprotective IGF-1 [23]. Yet, the role of chymase in promoting cardiomyocyte apoptosis can be multifaceted. TGF-β receptor expression and activation on cardiomyocytes can promote these cells undergoing apoptosis by activating downstream p38 MAP kinase and Smad signaling pathways [54–56]. Reduced TGF-β signaling in the myocardium from *Mcpt4*$^{-/-}$ mice but not in fibroblasts from these mice suggests impaired TGF-β signaling in cardiomyocytes from *Mcpt4*$^{-/-}$ mice. Our study also suggests that mMCP4 promotes cardiomyocyte apoptosis by regulating cathepsin activity that involves in tBid production [36,40,41]. Reduced expression of CatS, CatK, CatL, and CatB along with reduced Bax and tBid in cardiomyocytes from *Mcpt4*$^{-/-}$ mice supports this possibility. Cardiomyocyte death is an important signature of post-MI myocardium. mMCP4 expression did not affect post-MI myocardial expression of collagen and α-SMA, suggesting that mMCP4 contributed to post-MI cardiac dysfunction by promoting cardiomyocyte apoptosis but not fibrosis. Therefore, post-MI cardiac dysfunction may not have to associate with myocardial expression of collagen or α-SMA [57,58].

In summary, this study established the direct participation of a chymase ortholog in cardiac dysfunction following coronary artery ligation by affecting myocardial inflammatory cell content, regulating cardiac tissue MMP and cathepsin protease expression and activities, and promoting cardiomyocyte death. Chymase activity in TGF-β signaling may be cell type-dependent. In mouse fibroblasts, chymase played a minimal role in TGF-β signaling, which may explain negligible changes in cardiac fibrosis in mMCP4-deficient hearts. Nevertheless, together with prior studies from mMCP4-deficeint mice and chymase inhibitors, chymase inhibition may improve healing and function of the heart following an ischemic insult.

Supplementary Material

Refer to Web version on PubMed Central for supplementary material.

Acknowledgements

The authors thank Eugenia Shvartz for her technical assistance.

Funding

This work was supported by awards from the American Heart Association (17POST33670564 to C.-L.L.), the National Natural Science Foundation of China (81570274 to J.Z.), University-College Joint Cultivation Fund of Zhengzhou University, (2016_BSTDJJ-19 to J.Z.), National Institute of Health [HL080472 to PL, HL123568 and HL60942 to G.-P.S.], and the RRM Charitable Fund to P.L.

References

[1]. Shi GP, Bot I, Kovanen PT. Mast cells in human and experimental cardiometabolic diseases. Nat Rev Cardiol 2015;12:643–658. [PubMed: 26259935]

[2]. Pejler G, Ronnberg E, Waern I, Wernersson S. Mast cell proteases: multifaceted regulators of inflammatory disease. Blood 2010;115:4981–4990. [PubMed: 20233968]

[3]. Pejler G, Abrink M, Ringvall M, Wernersson S. Mast cell proteases. Adv Immunol 2007;95:167–255. [PubMed: 17869614]

[4]. Yusof M, Kamada K, Gaskin FS, Korthuis RJ. Angiotensin II mediates postischemic leukocyte-endothelial interactions: role of calcitonin gene-related peptide. Am J Physiol Heart Circ Physiol 2007;292:H3032–3037. [PubMed: 17307998]

[5]. Nguyen SD, Maaninka K, Lappalainen J, Nurmi K, Metso J, Oorni K, Navab M, Fogelman AM, Jauhiainen M, Lee-Rueckert M, Kovanen PT. Carboxyl-Terminal Cleavage of Apolipoprotein A-I by Human Mast Cell Chymase Impairs Its Anti-Inflammatory Properties. Arterioscler Thromb Vasc Biol 2016;36:274–284. [PubMed: 26681753]

[6]. Miyazaki M, Wada T, Shiota N, Takai S. Effect of an angiotensin II receptor antagonist, candesartan cilexetil, on canine intima hyperplasia after balloon injury. J Hum Hypertens 1999;13 Suppl 1:S21–25; discussion S33–24. [PubMed: 10076917]

[7]. Miyazaki M, Takai S, Jin D, Muramatsu M. Pathological roles of angiotensin II produced by mast cell chymase and the effects of chymase inhibition in animal models. Pharmacol Ther 2006;112:668–676. [PubMed: 16837049]

[8]. Schieffer B, Schieffer E, Hilfiker-Kleiner D, Hilfiker A, Kovanen PT, Kaartinen M, Nussberger J, Harringer W, Drexler H. Expression of angiotensin II and interleukin 6 in human coronary atherosclerotic plaques: potential implications for inflammation and plaque instability. Circulation 2000;101:1372–1378. [PubMed: 10736279]

[9]. Gruber BL, Marchese MJ, Suzuki K, Schwartz LB, Okada Y, Nagase H, Ramamurthy NS. Synovial procollagenase activation by human mast cell tryptase dependence upon matrix metalloproteinase 3 activation. J Clin Invest 1989;84:1657–1662. [PubMed: 2553780]

[10]. Saarinen J, Kalkkinen N, Welgus HG, Kovanen PT. Activation of human interstitial procollagenase through direct cleavage of the Leu83-Thr84 bond by mast cell chymase. J Biol Chem 1994;269:18134–18140. [PubMed: 8027075]

[11]. Taipale J, Lohi J, Saarinen J, Kovanen PT, Keski-Oja J. Human mast cell chymase and leukocyte elastase release latent transforming growth factor-beta 1 from the extracellular matrix of cultured human epithelial and endothelial cells. J Biol Chem 1995;270:4689–4696. [PubMed: 7876240]

[12]. Takai S, Jin D, Sakaguchi M, Katayama S, Muramatsu M, Sakaguchi M, Matsumura E, Kim S, Miyazaki M. A novel chymase inhibitor, 4-[1-([bis-(4-methyl-phenyl)methyl]-carbamoyl)3-(2-ethoxy-benzyl)-4-oxo-azetidin e-2-yloxy]-benzoic acid (BCEAB), suppressed cardiac fibrosis in cardiomyopathic hamsters. J Pharmacol Exp Ther 2003;305:17–23. [PubMed: 12649348]

[13]. Ihara M, Urata H, Shirai K, Ideishi M, Hoshino F, Suzumiya J, Kikuchi M, Arakawa K. High cardiac angiotensin-II-forming activity in infarcted and non-infarcted human myocardium. Cardiology 2000;94:247–253. [PubMed: 11326146]

[14]. Shiota N, Jin D, Takai S, Kawamura T, Koyama M, Nakamura N, Miyazaki M. Chymase is activated in the hamster heart following ventricular fibrosis during the chronic stage of hypertension. FEBS Lett 1997;406:301–304. [PubMed: 9136906]

[15]. Inoue N, Muramatsu M, Jin D, Takai S, Hayashi T, Katayama H, Kitaura Y, Tamai H, Miyazaki M. Effects of chymase inhibitor on angiotensin II-induced abdominal aortic aneurysm development in apolipoprotein E-deficient mice. Atherosclerosis 2009;204:359–364. [PubMed: 18996524]

[16]. Wei CC, Hase N, Inoue Y, Bradley EW, Yahiro E, Li M, Naqvi N, Powell PC, Shi K, Takahashi Y, Saku K, Urata H, Dell'italia LJ, Husain A. Mast cell chymase limits the cardiac efficacy of Ang I-converting enzyme inhibitor therapy in rodents. J Clin Invest 2010;120:1229–1239. [PubMed: 20335663]

[17]. Hoshino F, Urata H, Inoue Y, Saito Y, Yahiro E, Ideishi M, Arakawa K, Saku K. Chymase inhibitor improves survival in hamsters with myocardial infarction. J Cardiovasc Pharmacol 2003;41 Suppl 1:S11–18. [PubMed: 12688390]

[18]. Jin D, Takai S, Yamada M, Sakaguchi M, Miyazaki M. Beneficial effects of cardiac chymase inhibition during the acute phase of myocardial infarction. Life Sci 2002;71:437–446. [PubMed: 12044843]

[19]. Jin D, Takai S, Yamada M, Sakaguchi M, Kamoshita K, Ishida K, Sukenaga Y, Miyazaki M. Impact of chymase inhibitor on cardiac function and survival after myocardial infarction. Cardiovasc Res 2003;60:413–420. [PubMed: 14613871]

[20]. Kanemitsu H, Takai S, Tsuneyoshi H, Nishina T, Yoshikawa K, Miyazaki M, Ikeda T, Komeda M. Chymase inhibition prevents cardiac fibrosis and dysfunction after myocardial infarction in rats. Hypertens Res 2006;29:57–64. [PubMed: 16715654]

[21]. Zheng J, Wei CC, Hase N, Shi K, Killingsworth CR, Litovsky SH, Powell PC, Kobayashi T, Ferrario CM, Rab A, Aban I, Collawn JF, Dell'Italia LJ. Chymase mediates injury and mitochondrial damage in cardiomyocytes during acute ischemia/reperfusion in the dog. PLoS One 2014;9:e94732. [PubMed: 24733352]

[22]. Sun J, Zhang J, Lindholt JS, Sukhova GK, Liu J, He A, Abrink M, Pejler G, Stevens RL, Thompson RW, Ennis TL, Gurish MF, Libby P, Shi GP. Critical role of mast cell chymase in mouse abdominal aortic aneurysm formation. Circulation 2009;120:973–982. [PubMed: 19720934]

[23]. Tejada T, Tan L, Torres RA, Calvert JW, Lambert JP, Zaidi M, Husain M, Berce MD, Naib H, Pejler G, Abrink M, Graham RM, Lefer DJ, Naqvi N, Husain A. IGF-1 degradation by mouse mast cell protease 4 promotes cell death and adverse cardiac remodeling days after a myocardial infarction. Proc Natl Acad Sci U S A 2016;113:6949–6954. [PubMed: 27274047]

[24]. Dai W, Kloner RA. Cardioprotection of insulin-like growth factor-1 during reperfusion therapy: what is the underlying mechanism or mechanisms? Circ Cardiovasc Interv 2011;4:311–313. [PubMed: 21846897]

[25]. Chen H, Wang J, Xiang MX, Lin Y, He A, Jin CN, Guan J, Sukhova GK, Libby P, Wang JA, Shi GP. Cathepsin S-mediated fibroblast trans-differentiation contributes to left ventricular remodelling after myocardial infarction. Cardiovasc Res 2013;100:84–94. [PubMed: 23771947]

[26]. Sun J, Sukhova GK, Wolters PJ, Yang M, Kitamoto S, Libby P, MacFarlane LA, Mallen-St Clair J, Shi GP. Mast cells promote atherosclerosis by releasing proinflammatory cytokines. Nat Med 2007;13:719–724. [PubMed: 17546038]

[27]. Sales VL, Sukhova GK, Lopez-Ilasaca MA, Libby P, Dzau VJ, Pratt RE. Angiotensin type 2 receptor is expressed in murine atherosclerotic lesions and modulates lesion evolution. Circulation. 2005;112(21):3328–36. [PubMed: 16286588]

[28]. Shi GP, Villadangos JA, Dranoff G, Small C, Gu L, Haley KJ, Riese R, Ploegh HL, Chapman HA. Cathepsin S required for normal MHC class II peptide loading and germinal center development. Immunity 1999;10:197–206. [PubMed: 10072072]

[29]. Li D, Wu J, Bai Y, Zhao X, Liu L. Isolation and culture of adult mouse cardiomyocytes for cell signaling and in vitro cardiac hypertrophy. J Vis Exp 2014.

[30]. Wu J, Li D, Du L, Baldawi M, Gable ME, Askari A, Liu L. Ouabain prevents pathological cardiac hypertrophy and heart failure through activation of phosphoinositide 3-kinase alpha in mouse. Cell Biosci 2015;5:64. [PubMed: 26587223]

[31]. Fang KC, Raymond WW, Lazarus SC, Caughey GH. Dog mastocytoma cells secrete a 92-kD gelatinase activated extracellularly by mast cell chymase. J Clin Invest 1996;97:1589–1596. [PubMed: 8601622]

[32]. Shi GP, Webb AC, Foster KE, Knoll JH, Lemere CA, Munger JS, Chapman HA. Human cathepsin S: chromosomal localization, gene structure, and tissue distribution. J Biol Chem 1994;269:11530–11536. [PubMed: 8157683]

[33]. Takai S, Jin D, Chen H, Li W, Yamamoto H, Yamanishi K, Miyazaki M, Higashino H, Yamanishi H, Okamura H. Chymase inhibition improves vascular dysfunction and survival in stroke-prone spontaneously hypertensive rats. J Hypertens 2014;32:1637–1648; discussion 1649. [PubMed: 24886822]

[34]. Hara M, Matsumori A, Ono K, Kido H, Hwang MW, Miyamoto T, Iwasaki A, Okada M, Nakatani K, Sasayama S. Mast cells cause apoptosis of cardiomyocytes and proliferation of other intramyocardial cells in vitro. Circulation 1999;100:1443–1449. [PubMed: 10500047]

[35]. Christensen J, Shastri VP. Matrix-metalloproteinase-9 is cleaved and activated by cathepsin K. BMC Res Notes. 2015;8:322. [PubMed: 26219353]

[36]. Liu CL, Guo J, Zhang X, Sukhova GK, Libby P, Shi GP. Cysteine protease cathepsins in cardiovascular disease: from basic research to clinical trials. Nat Rev Cardiol. 2018;15:351–70. [PubMed: 29679024]

[37]. Kurisaki A, Kose S, Yoneda Y, Heldin CH, Moustakas A. Transforming growth factor-beta induces nuclear import of Smad3 in an importin-beta1 and Ran-dependent manner. Mol Biol Cell 2001;12:1079–1091. [PubMed: 11294908]

[38]. Dai F, Lin X, Chang C, Feng XH. Nuclear export of Smad2 and Smad3 by RanBP3 facilitates termination of TGF-beta signaling. Dev Cell 2009;16:345–357. [PubMed: 19289081]

[39]. van Empel VP, Bertrand AT, Hofstra L, Crijns HJ, Doevendans PA, De Windt LJ. Myocyte apoptosis in heart failure. Cardiovasc Res 2005;67:21–29. [PubMed: 15896727]

[40]. Droga-Mazovec G, Bojic L, Petelin A, Ivanova S, Romih R, Repnik U, Salvesen GS, Stoka V, Turk V, Turk B. Cysteine cathepsins trigger caspase-dependent cell death through cleavage of bid and antiapoptotic Bcl-2 homologues. J Biol Chem 2008;283:19140–19150. [PubMed: 18469004]

[41]. Blomgran R, Zheng L, Stendahl O. Cathepsin-cleaved Bid promotes apoptosis in human neutrophils via oxidative stress-induced lysosomal membrane permeabilization. J Leukoc Biol 2007;81:1213–1223. [PubMed: 17264306]

[42]. Kosanovic D, Luitel H, Dahal BK, Cornitescu T, Janssen W, Danser AH, Garrelds IM, De Mey JG, Fazzi G, Schiffers P, Iglarz M, Fischli W, Ghofrani HA, Weissmann N, Grimminger F, Seeger W, Reiss I, Schermuly RT. Chymase: a multifunctional player in pulmonary hypertension associated with lung fibrosis. Eur Respir J 2015;46:1084–1094. [PubMed: 26113671]

[43]. Houde M, Jamain MD, Labonte J, Desbiens L, Pejler G, Gurish M, Takai S, D'Orleans-Juste P. Pivotal role of mouse mast cell protease 4 in the conversion and pressor properties of Big-endothelin-1. J Pharmacol Exp Ther 2013;346:31–37. [PubMed: 23596057]

[44]. Sun J, Sukhova GK, Zhang J, Chen H, Sjoberg S, Libby P, Xiang M, Wang J, Peters C, Reinheckel T, Shi GP. Cathepsin L activity is essential to elastase perfusion-induced abdominal aortic aneurysms in mice. Arterioscler Thromb Vasc Biol 2011;31:2500–2508. [PubMed: 21868704]

[45]. Wolters PJ, Pham CT, Muilenburg DJ, Ley TJ, Caughey GH. Dipeptidyl peptidase I is essential for activation of mast cell chymases, but not tryptases, in mice. J Biol Chem 2001;276:18551–18556. [PubMed: 11279033]

[46]. Gu Y, Lewis DF, Alexander JS, Wang Y. Upregulation of cathepsin C expression contributes to endothelial chymase activation in preeclampsia. Hypertens Res 2017;40:976–981. [PubMed: 28878298]

[47]. Koitabashi N, Danner T, Zaiman AL, Pinto YM, Rowell J, Mankowski J, Zhang D, Nakamura T, Takimoto E, Kass DA. Pivotal role of cardiomyocyte TGF-beta signaling in the murine pathological response to sustained pressure overload. J Clin Invest 2011;121:2301–2312. [PubMed: 21537080]

[48]. Schultz Jel J, Witt SA, Glascock BJ, Nieman ML, Reiser PJ, Nix SL, Kimball TR, Doetschman T. TGF-beta1 mediates the hypertrophic cardiomyocyte growth induced by angiotensin II. J Clin Invest 2002;109:787–796. [PubMed: 11901187]

[49]. Rainer PP, Hao S, Vanhoutte D, Lee DI, Koitabashi N, Molkentin JD, Kass DA. Cardiomyocyte-specific transforming growth factor beta suppression blocks neutrophil infiltration, augments multiple cytoprotective cascades, and reduces early mortality after myocardial infarction. Circ Res 2014;114:1246–1257. [PubMed: 24573206]

[50]. Pan LJ, Wang X, Ling Y, Gong H. MiR-24 alleviates cardiomyocyte apoptosis after myocardial infarction via targeting BIM. Eur Rev Med Pharmacol Sci 2017;21:3088–3097. [PubMed: 28742197]

[51]. Diwan A, Krenz M, Syed FM, Wansapura J, Ren X, Koesters AG, Li H, Kirshenbaum LA, Hahn HS, Robbins J, Jones WK, Dorn GW. Inhibition of ischemic cardiomyocyte apoptosis through targeted ablation of Bnip3 restrains postinfarction remodeling in mice. J Clin Invest 2007;117:2825–2833. [PubMed: 17909626]

[52]. Wang L, Ma W, Markovich R, Chen JW, Wang PH. Regulation of cardiomyocyte apoptotic signaling by insulin-like growth factor I. Circ Res 1998;83:516–522. [PubMed: 9734474]

[53]. Maldonado C, Cea P, Adasme T, Collao A, Diaz-Araya G, Chiong M, Lavandero S. IGF-1 protects cardiac myocytes from hyperosmotic stress-induced apoptosis via CREB. Biochem Biophys Res Commun 2005;336:1112–1118. [PubMed: 16168389]

[54]. Heger J, Warga B, Meyering B, Abdallah Y, Schluter KD, Piper HM, Euler G. TGFbeta receptor activation enhances cardiac apoptosis via SMAD activation and concomitant NO release. J Cell Physiol 2011;226:2683–2690. [PubMed: 21792926]

[55]. Sun F, Li X, Duan WQ, Tian W, Gao M, Yang J, Wu XY, Huang D, Xia W, Han YN, Wang JX, Liu YX, Dong CJ, Zhao D, Ban T, Chu WF. Transforming Growth Factor-beta Receptor III is a Potential Regulator of Ischemia-Induced Cardiomyocyte Apoptosis. J Am Heart Assoc 2017;6.

[56]. Schneiders D, Heger J, Best P, Michael Piper H, Taimor G. SMAD proteins are involved in apoptosis induction in ventricular cardiomyocytes. Cardiovasc Res 2005;67:87–96. [PubMed: 15949472]

[57]. Van Aelst LN, Voss S, Carai P, Van Leeuwen R, Vanhoutte D, Sanders-van Wijk S, et al. Osteoglycin prevents cardiac dilatation and dysfunction after myocardial infarction through infarct collagen strengthening. Circ Res. 2015;116:425–36. [PubMed: 25520363]

[58]. McSweeney SJ, Hadoke PW, Kozak AM, Small GR, Khaled H, Walker BR, et al. Improved heart function follows enhanced inflammatory cell recruitment and angiogenesis in 11betaHSD1-deficient mice post-MI. Cardiovasc Res. 2010;88:159–67. [PubMed: 20495186]

Highlights

- In post-MI mice, mMCP4 is expressed in cardiomyocytes from the infarct region. Deficiency of mMCP4 reduces infarct size, protects cardiac dysfunction and body weight drop, and affects myocardium inflammatory cell accumulation, but does not change survival and LV morphology or fibrosis.
- mMCP4-deficiency reduces post-MI heart cardiomyocyte apoptosis and myocardial TGF-β signaling, protects cultured cardiomyocytes from H_2O_2-induced apoptosis, but does not affect TGF-β signaling in cultured cardiac fibroblasts.
- mMCP4-deficiency reduces MMP activity and cathepsin expression from post-MI heart and in cultured macrophages and T cells.

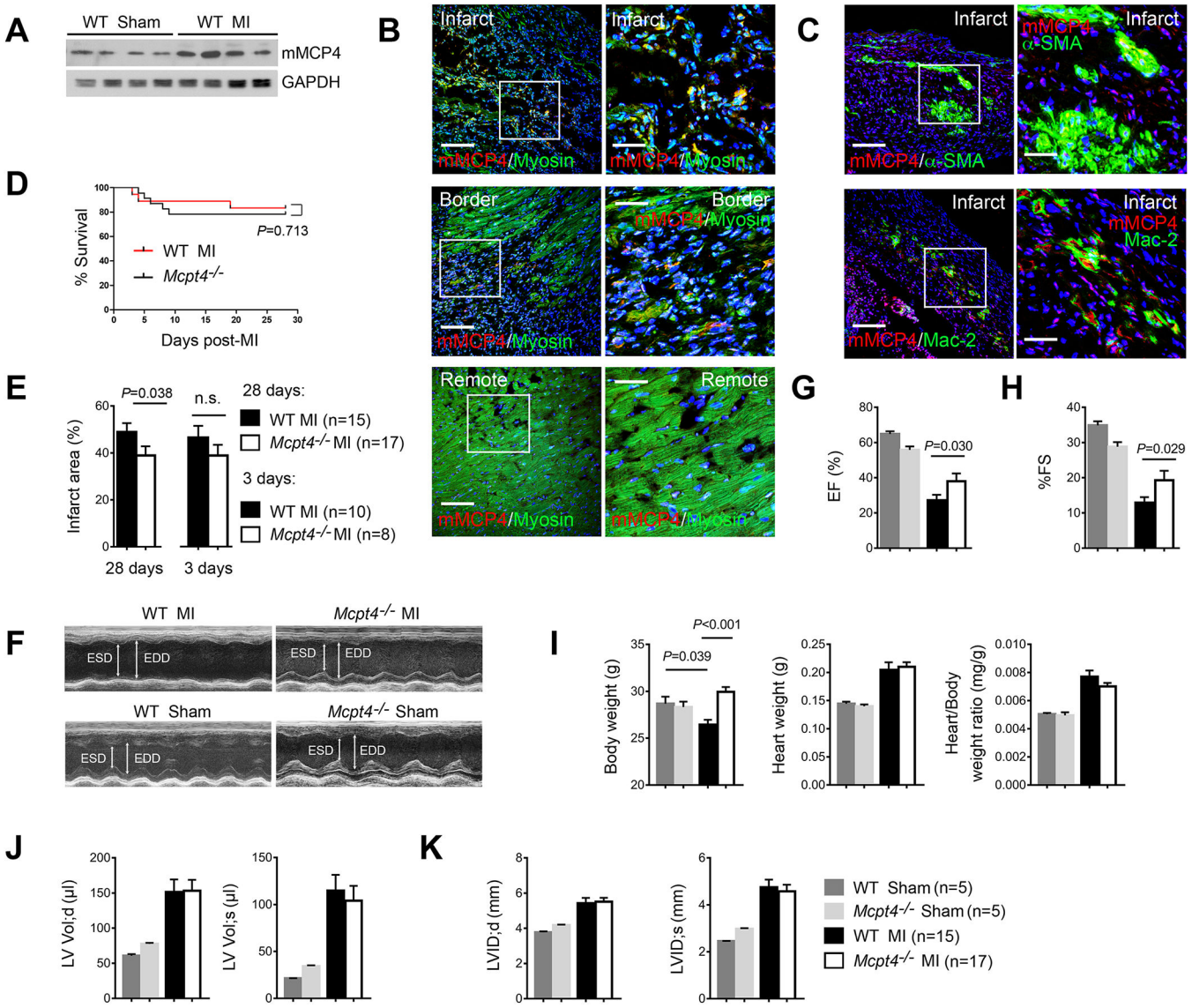

Fig. 1.

Chymase mMCP4 expression and function in mice after MI injury. **A.** Western blot analysis of mouse chymase mMCP4 expression in sham-operated and 28 days post-MI hearts from WT mice. **B.** Immunofluorescent double staining colocalized mMCP4-positive cells to myosin heavy chain-positive cardiomyocytes in the infarct, border, and remote regions in WT mice at 28 days post-MI. **C**. Immunofluorescent double staining showed mMCP4 expression in α-SMA-positive fibroblasts and Mac-2-positive macrophages in the infarct regions from 28 days post-MI heart. Scale: 200 μm, inset scale: 70 μm. **D.** Mortality rate of both WT and *Mcpt4*$^{-/-}$ mice during the course of 28 days of post-MI recovery. Kaplan-Meier survival analysis with log-rank test. **E.** Infarct sizes of both WT and *Mcpt4*$^{-/-}$ mice at 3 days and 28 days post-MI. Representative M-mode echocardiography images (**F**), ejection fraction (EF) (**G**), fractional shortening (FS) (**H**), body weight, heart weight, and heart-to-body weight ratio (**I**), LV diastole and systole volumes (**J**), and LV diastole and systole internal diameters (**K**) of WT and *Mcpt4*$^{-/-}$ mice at 28 days after sham operation or MI. The

mouse numbers and genotypes are indicated in the legends. $P<0.05$ was considered statistically significant, independent *t*-test or one-way ANOVA with post-hoc Bonferroni test. Data are mean±SEM.

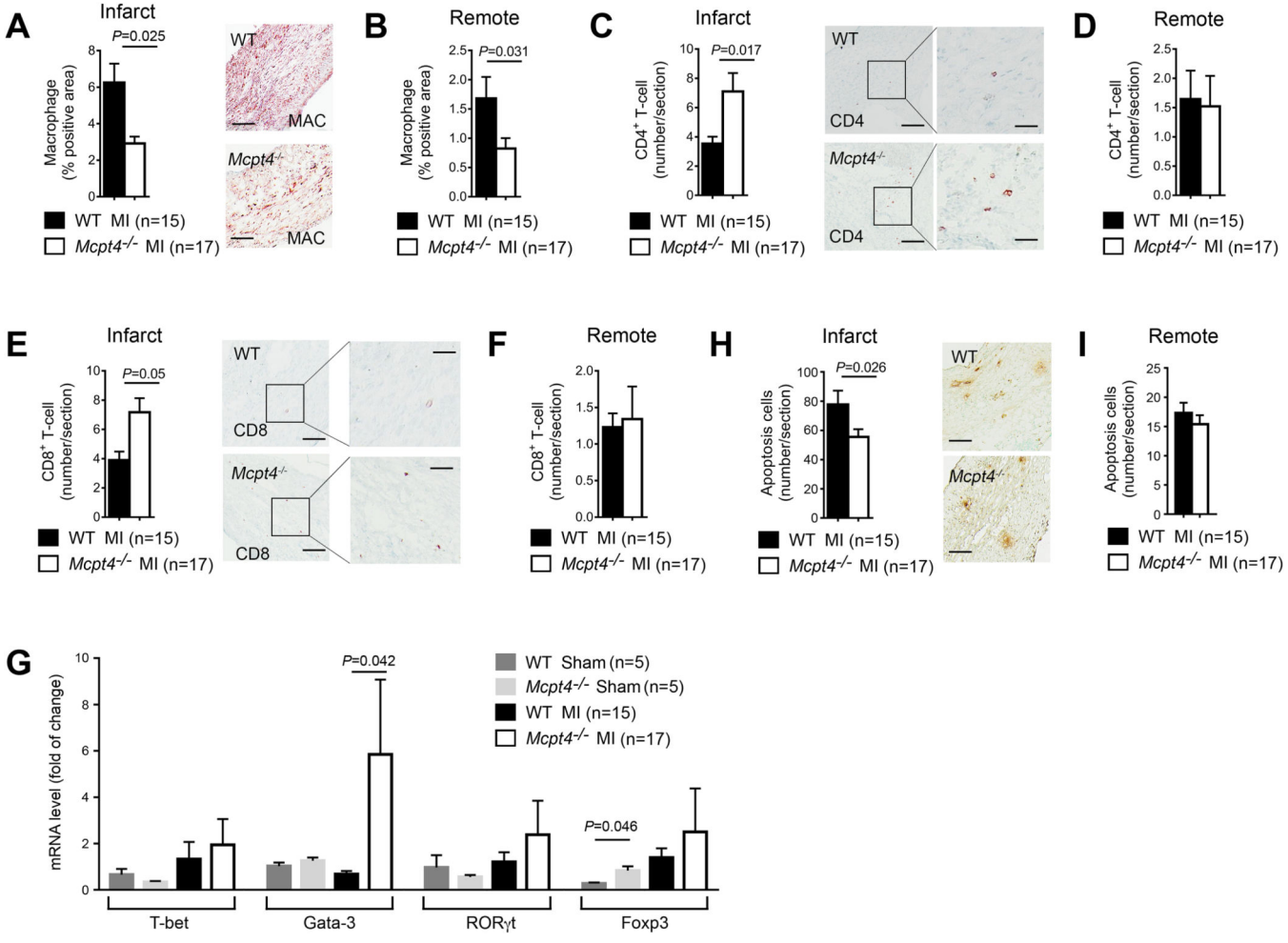

Fig. 2.

Post-MI myocardium inflammatory cell infiltration and cell apoptosis. Immunostaining of Mac-3-positive macrophages in infarct (**A**) and remote (**B**) areas, $CD4^+$ T cells in infarct (**C**) and remote (**D**) areas, and $CD8^+$ T cells in infarct (**E**) and remote (**F**) areas of both WT and *Mcpt4*$^{-/-}$ mice at 28 days post-MI. **G.** RT-PCR analysis of relative mRNA level of T-bet, Gata-3, RORγt, and Foxp3 in the same infarct regions as above. TUNEL staining of apoptotic cells in infarct (**H**) and remote (**I**) regions from above. The numbers of mice in each group are shown in the legend. Scale: 150 μm, inset scale: 50 μm. $P<0.05$ was considered statistically significant, independent *t*-test or one-way ANOVA with post-hoc Bonferroni test. Data are mean±SEM.

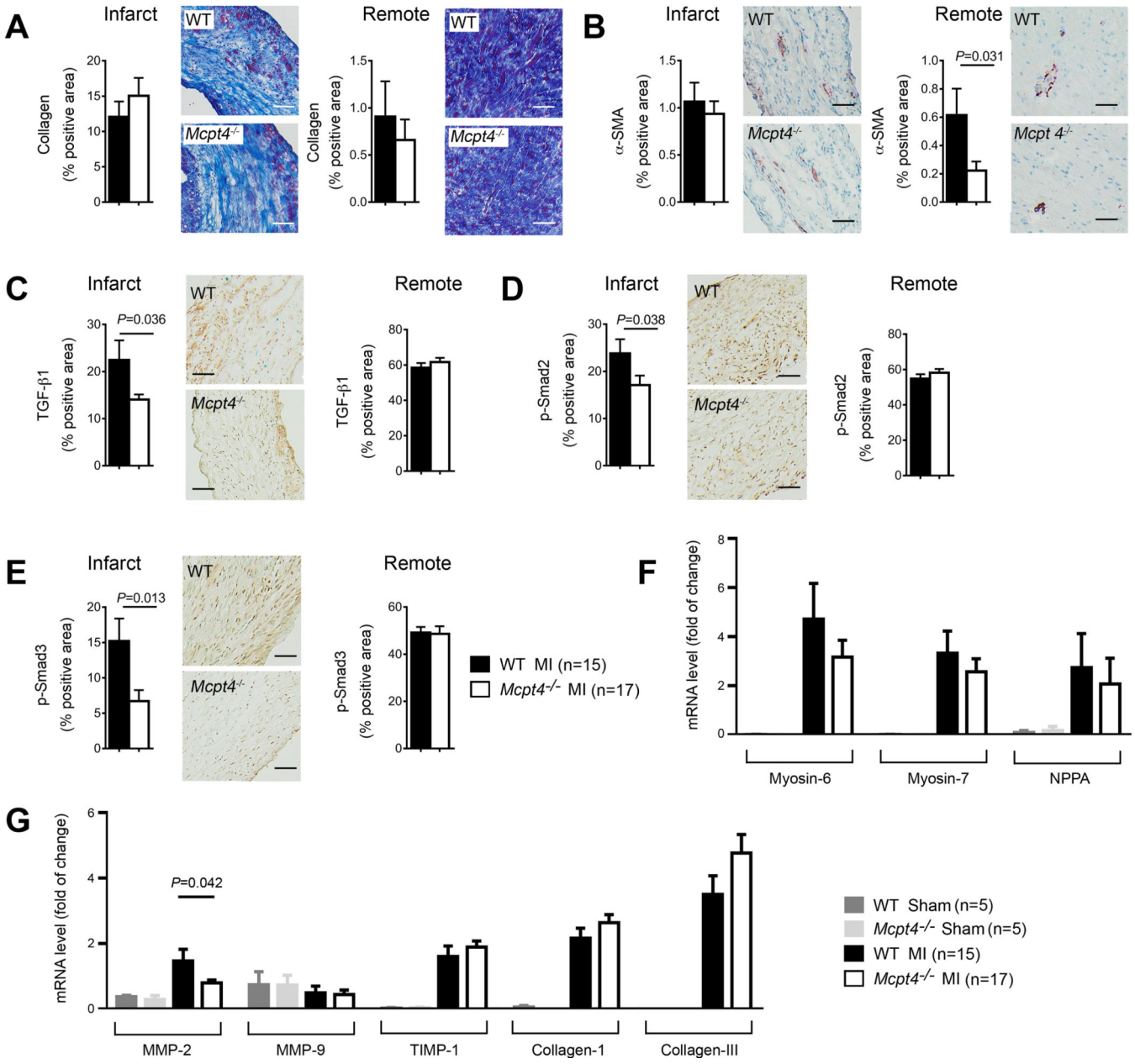

Fig. 3.

Post-MI myocardial fibrosis and TGF-β signaling in WT and *Mcpt4*$^{-/-}$ mice. **A.** Masson's trichrome staining of collagen deposition in the infarct and remote regions. **B.** α-SMA-positive areas in the infarct and remote regions. Immunostaining of TGF-β1 (**C**), p-Smad2 (**D**), and p-Smad3 (**E**) in both infarct and remote regions at 28 days post-MI. Scale: 150 μm. **F/G**. RT-PCR analysis of relative mRNA levels of myosin-6, myosin-7, NPPA, MMP-2, MMP-9, TIMP-1, collagen-I and collagen-III in the same infarct regions as above. The number and genotype of mice in each group are shown in the legend. $P<0.05$ was considered statistically significant, independent *t*-test. Data are mean±SEM.

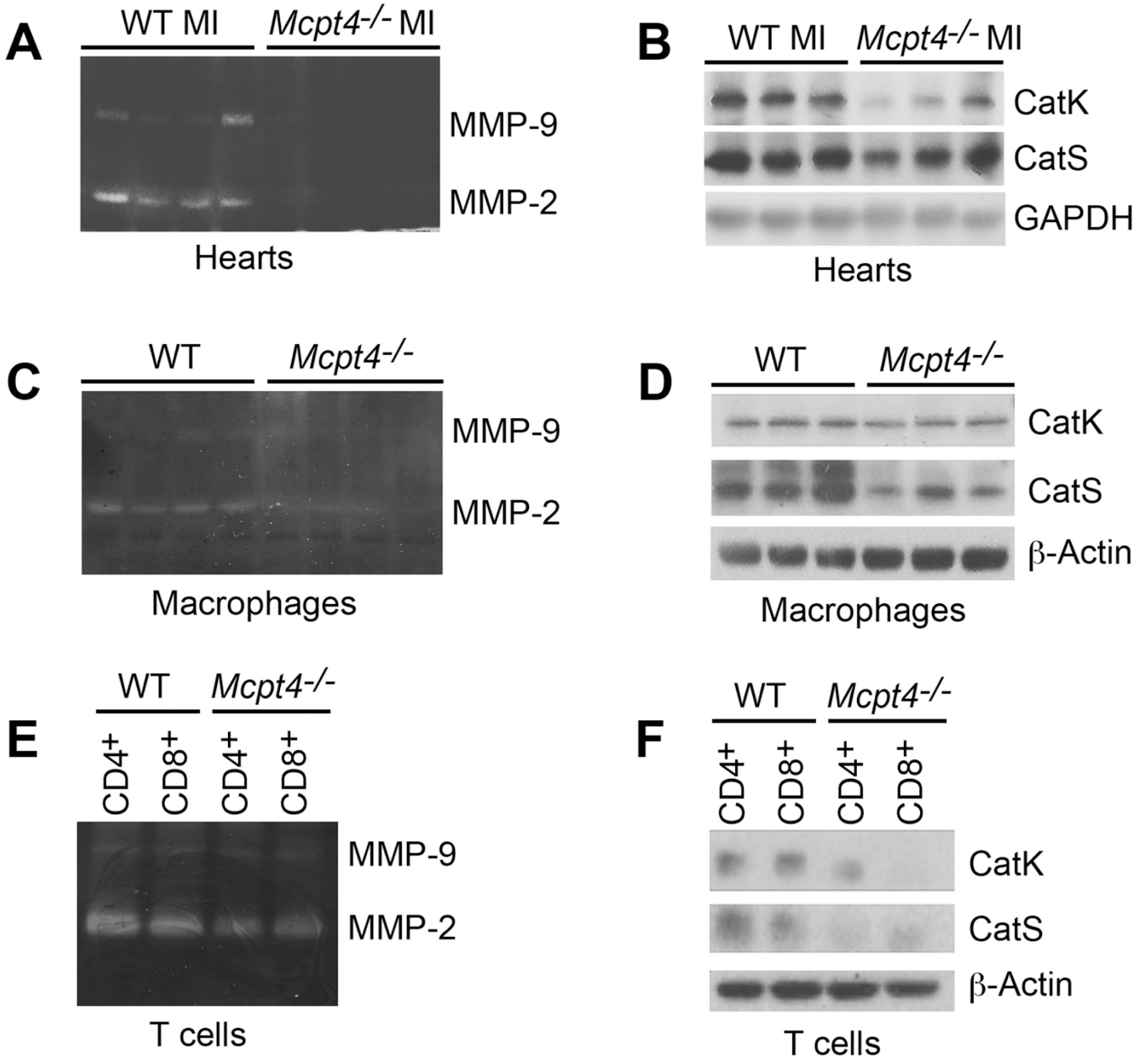

Fig. 4.

MMP zymography and cysteinyl cathepsin immunoblot analysis in post-MI myocardium and inflammatory cells. MMP zymography (**A**) and cathepsin immunoblot analysis (**B**) in myocardial tissue extracts from WT and *Mcpt4*$^{-/-}$ MI mice at 28 days post-MI. MMP zymography (**C**/**E**) and cathepsin immunoblot analysis (**D**/**F**) in bone marrow-derived macrophages (**C**/**D**) and splenic CD4^{+} and CD8^{+} T cells (**E**/**F**) from WT and *Mcpt4*$^{-/-}$ MI mice. In immunoblot analyses, the same blots were reprobed for β-Actin to ensure equal protein loading. Data are representative of three independent experiments.

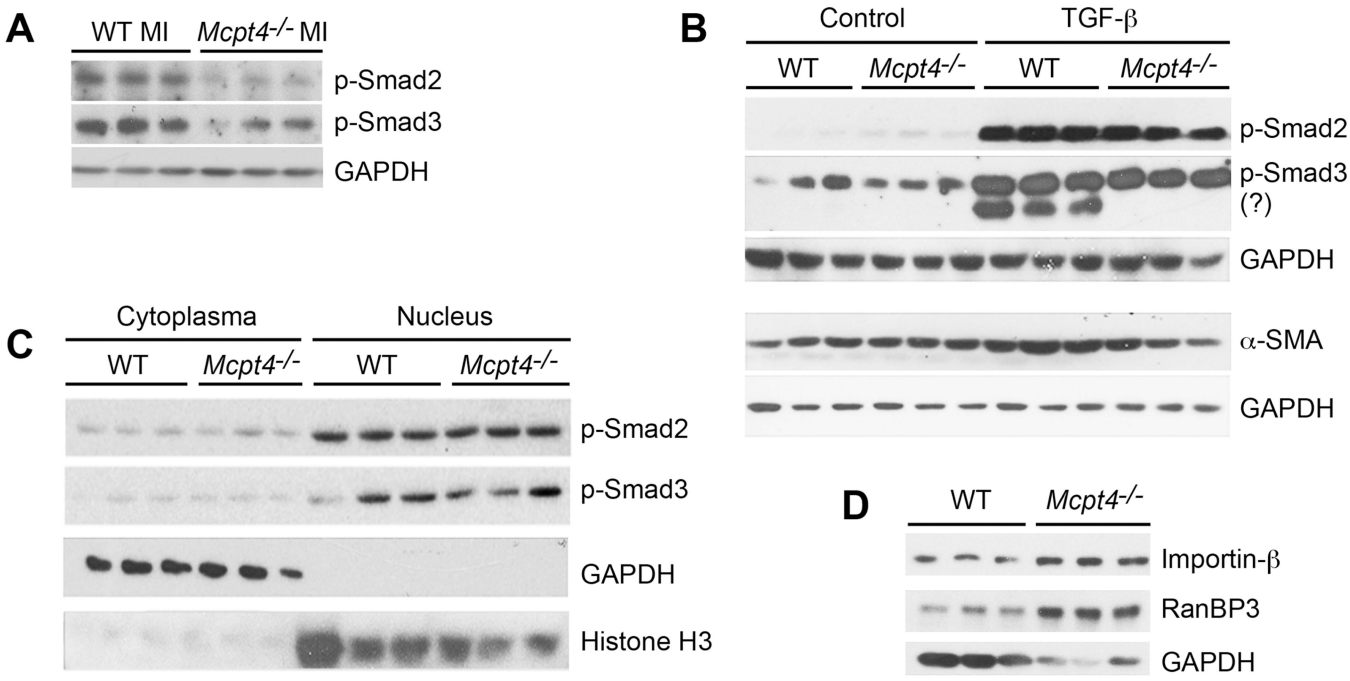

Fig. 5.

TGF-β1 signaling in mouse cardiac tissue extracts and cardiac fibroblasts. **A**. Immunoblot analysis of p-Smad2 and p-Smad3 in cardiac tissue extracts from WT and *Mcpt4*$^{-/-}$ mice at 28 days post-MI. **B.** Immunoblot analysis of p-Smad2, p-Smad3, and α-SMA in fibroblasts from WT and *Mcpt4*$^{-/-}$ mice with and without TGF-β stimulation for 30 min (for p-Smad2 and p-Smad3) or 36 hours (for α-SMA). **C.** Immunoblot analysis of p-Smad2 and p-Smad3 in cytosolic and nuclear fractions of fibroblasts from WT and *Mcpt4*$^{-/-}$ mice. The same blot was reprobed for GAPDH and histone H3 to ensure cytosol and nucleus separation. **D**. Immunoblot analysis of nuclear membrane importer importin-β and exporter RanBP3 in fibroblasts from WT and *Mcpt4*$^{-/-}$ mice. The same blots were reprobed for GAPDH to examine equal protein loading in panels **A**, **B**, and **D**. Data are representative of three independent experiments.

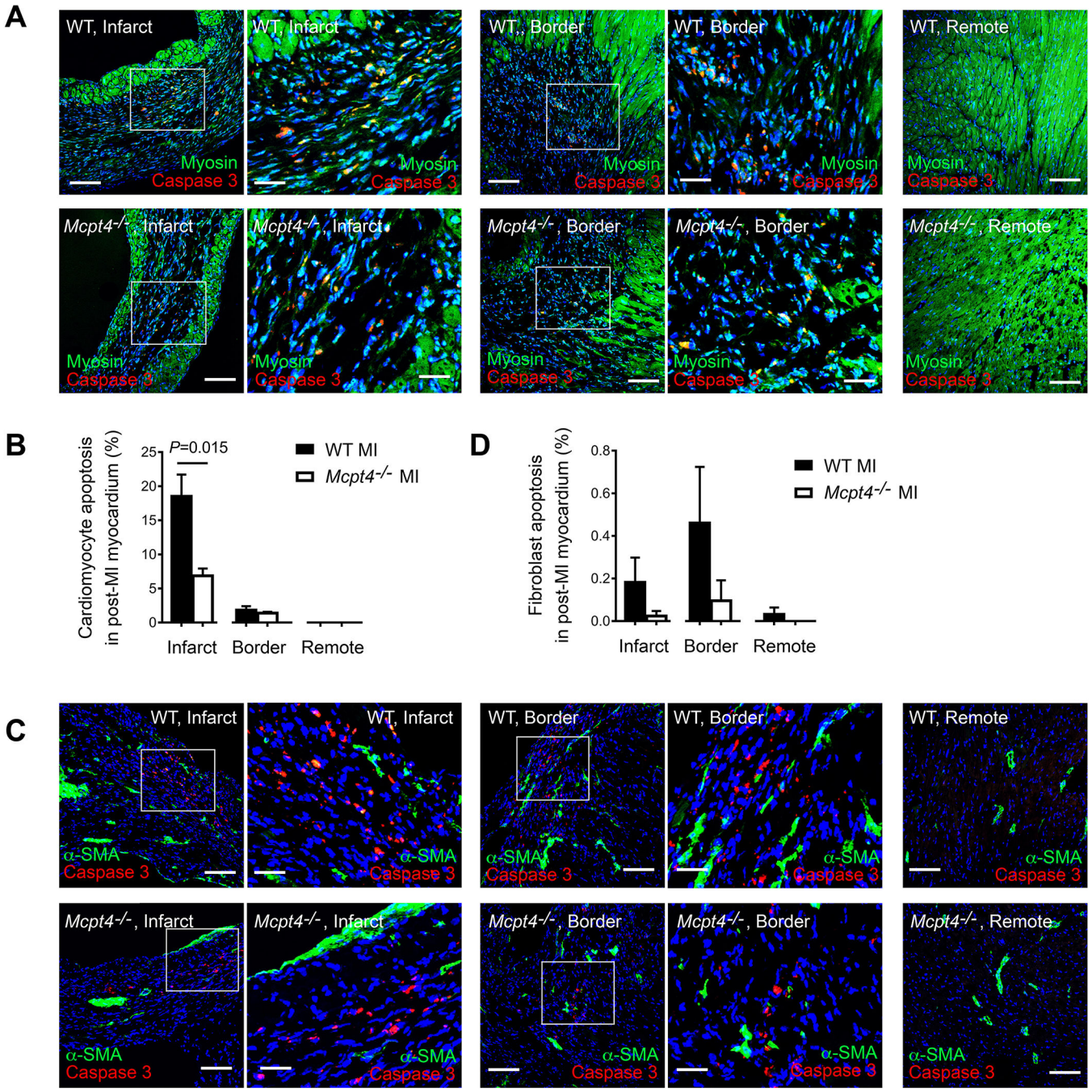

Fig. 6.

Cell apoptosis in post-MI myocardium. **A**. Immunofluorescent double staining colocalized cleaved caspase 3-positive cells to myosin heavy chain-positive cardiomyocytes in infarct, border, and remote regions from WT (top panels) and *Mcpt4*$^{-/-}$ mice (bottom panels) at 28 days post-MI. **B.** Quantification of apoptotic cardiomyocytes in infarct, border, and remote regions. **C**. Immunofluorescent double staining colocalized cleaved caspase 3-positive cells to α-SMA-positive fibroblasts in infarct, border, and remote regions from WT (top panels) and *Mcpt4*$^{-/-}$ mice (bottom panels) at 28 days post-MI. **D.** Quantification of fibroblast

apoptosis in infarct, border, and remote regions. Scale: 200 μm, inset scale: 70 μm. Data are representative of 6~8 specimens per genotype. $P<0.05$ was considered statistically significant, independent *t*-test. Data are mean±SEM.

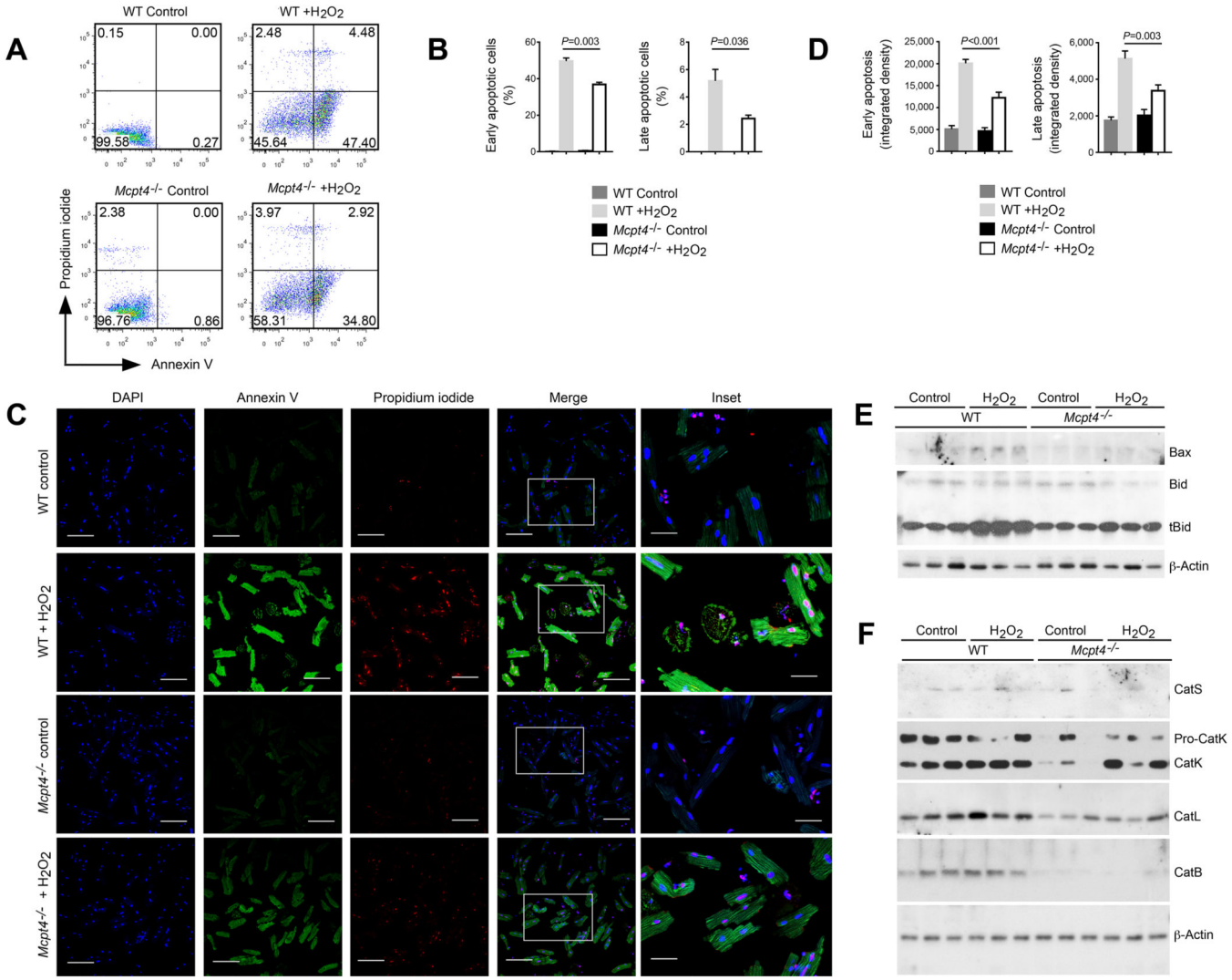

Figure 7

Fig. 7.

Role of mMCP4 in cardiomyocyte apoptosis. **A/B.** Representative FACS analysis and quantification of Annexin V^+PI^- early apoptotic cardiomyocytes and Annexin V^+PI^+ late apoptotic cardiomyocytes from WT and *Mcpt4*$^{-/-}$ mice after cells were treated with and without (Control) H_2O_2. **C/D.** Annexin V and PI immunofluorescent staining representative images and apoptosis quantification of cardiomyocytes from WT and *Mcpt4*$^{-/-}$ mice with and without 100 μM H_2O_2 treatment. Data are mean±SEM from six independent experiments. Scale: 200 μm, inset scale: 70 μm. **E.** Immunoblot analysis of Bax, Bid, and tBid in cardiomyocytes from WT and *Mcpt4*$^{-/-}$ mice after cells were treated with or without H_2O_2. **F.** Immunoblot analysis of CatS, CatK, CatL, and CatB in cardiomyocytes from WT and *Mcpt4*$^{-/-}$ mice after cells were treated with or without H_2O_2. The same blots were reprobed for β-Actin to ensure equal protein loading. Immunoblot data are representative of

three independent experiments. $P<0.05$ was considered statistically significant, independent *t*-test or one-way ANOVA with post-hoc Bonferroni test. Data are mean±SEM.